

Improving maps of ice-sheet surface elevation change using combined laser altimeter and stereoscopic elevation model data

J.F. LEVINSEN,¹ I.M. HOWAT,² C.C. TSCHERNING³

¹*Geodynamics Department, DTU Space, Elektrovej, Lyngby, Denmark
E-mail: jfl@space.dtu.dk*

²*School of Earth Sciences, Ohio State University, Columbus, OH, USA*

³*Niels Bohr Institute, University of Copenhagen, Copenhagen, Denmark*

ABSTRACT. We combine the complementary characteristics of laser altimeter data and stereoscopic digital elevation models (DEMs) to construct high-resolution (~100 m) maps of surface elevations and elevation changes over rapidly changing outlet glaciers in Greenland. Measurements from spaceborne and airborne laser altimeters have relatively low errors but are spatially limited to the ground tracks, while DEMs have larger errors but provide spatially continuous surfaces. The principle of our method is to fit the DEM surface to the altimeter point clouds in time and space to minimize the DEM errors and use that surface to extrapolate elevations away from altimeter flight lines. This reduces the DEM registration errors and fills the gap between the altimeter paths. We use data from ICESat and ATM as well as SPOT 5 DEMs from 2007 and 2008 and apply them to the outlet glaciers Jakobshavn Isbræ (JI) and Kangerdlugssuaq (KL). We find that the main trunks of JI and KL lowered at rates of 30–35 and 7–20 m a⁻¹, respectively. The rates decreased inland. The corresponding errors were 0.3–5.2 m a⁻¹ for JI and 0.3–5.1 m a⁻¹ for KL, with errors increasing proportionally with distance from the altimeter paths.

1. INTRODUCTION

The ice sheets have lost mass at an accelerating rate over the past decade, largely due to accelerated flow and drawdown at the margins. Several methods exist for observing surface elevation changes, including repeat laser and radar altimetry and stereoscopic digital elevation models (DEMs) from both airborne and satellite platforms (Howat and others, 2007; Berthier and Toutin, 2008; Thomas and others, 2009). Each method has its advantages and disadvantages: imagery-based DEMs provide a continuous surface and therefore wide coverage in both space and time but have relatively large errors; laser altimeters, in contrast, have a high accuracy, but measurements are limited to the flight paths of the satellite or airplane, which in turn are limited by logistics and cost. As the largest surface changes in Greenland are observed at the ice margin, where surface slopes are high and the topography rough, neither of these datasets alone can be used to map the changes with both high spatial coverage and low errors. Such measurements are, however, important, as accurate estimates of elevation changes can be used to infer knowledge of changes in the mass balance and eustatic sea level (Sørensen and others, 2011).

The goal of this work is to make use of the complementary characteristics of stereoscopic DEMs and laser altimeter data to improve the spatial coverage and resolution of surface elevation and elevation change estimates. This is done for two Greenland outlet glaciers, Jakobshavn Isbræ (JI) and Kangerdlugssuaq (KL), for the period 2007–08. We develop a method in which the DEM surface is co-registered to altimeter data by fitting DEM observations to the altimeter point cloud using a least-squares adjustment, thereby minimizing planimetric and elevation-dependent errors and removing biases. We test multiple methods for geostatistically interpolating the residuals between the altimeter and co-registered DEM data to further adjust the final surface and provide confidence intervals for our estimates. This allows the production of corrected DEMs with a high spatial

resolution even in areas of rough surface topography. Another important objective of this study is to examine how the confidence in surface elevation varies with distance from the altimeter flight paths, since this is essential information for planning future altimeter surveys. Several analyses have been conducted in which observations from the two sensors are combined: Carabajal and Harding (2005) used the Ice, Cloud and land Elevation Satellite (ICESat) to validate Shuttle Radar Topography Mission (STRM) C-band DEMs of the western United States by bilinear interpolation and comparison of the elevations, while Korona and others (2009) assumed ICESat data and SPOT 5 (Satellite Pour l'Observation de la Terre) DEMs from the SPIRIT (SPOT 5 stereoscopic survey of the Polar Ice: Reference Images and Topographies) campaign to be co-registered so the quality of the SPOT 5 observations could be tested. As such analyses can only provide reliable results if the co-registration works well, Schenk and others (2005) developed a method in which knowledge of terrain features (e.g. ridge crests and sudden change of slope) and a least-squares approach could be used to shift a DEM in space in order to minimize the Euclidean distance to the altimeter point cloud. Nuth and Kääb (2011) developed a method similar to ours for glaciated areas, although they did not make use of the information lying in the elevation difference between the altimeter and DEM surfaces, which varies with the topography and changes in the observed area. We thereby take their method one step further by employing geostatistical spatial interpolation techniques.

2. DATASETS

The DEMs are derived from SPOT 5 imagery obtained with the High Resolution Stereoscopic (HRS) sensor during the SPIRIT campaign (Korona and others, 2009). Due to the few repeat tracks from ICESat, these laser altimeter data are used in conjunction with lidar data from NASA's

Airborne Topographic Mapper (ATM) in order to ensure a high data coverage.

2.1. SPOT 5

The HRS sensor on board SPOT 5 is used to acquire stereoscopic pairs that can be combined to produce DEMs. Its two telescopes allow for along-track stereoscopy with a fore and aft view of 20° relative to nadir yielding a base-to-height (B/H) ratio of 0.8. The stereo pair consists of two images taken within a period of 90 s and covering an area of 600 km along-track × 120 km across-track. The short interval between the acquisition times ensures no significant temporal changes of the surface have occurred, while the use of a panchromatic band (0.48–0.7 m) minimizes the effects of shadows in areas of high relief. The resulting images have a pixel size of 5 m along-track × 10 m across-track with horizontal errors of 10–20 m, and elevation errors of 10–25 m depending on whether the surface is ice-covered or ice-free. The errors are caused, for example, by lack of radiometric contrasts in flat regions such as the snow-covered accumulation zone, steep slopes distorting the fore and aft view, or clouds moving and changing during the 90 s acquisition time. All of these break down the image correlation, thereby deteriorating the image quality (Bouillon and others, 2006; Berthier and Toutin, 2008; Korona and others, 2009). Following the fourth International Polar Year (IPY), the French Space Agency (CNES), SPOT Image and LEGOS (Laboratoire d'Etudes en Géophysique et Océanographie Spatiales) initiated the SPIRIT campaign. The goal was to create an archive of HRS images over polar ice and for specific areas to produce DEMs with a spatial resolution of 40 m and elevation errors on the decimeter level. The SPIRIT product consisted of two DEMs (for gentle and steep slopes, respectively), two reliability masks showing the correlation score and identifying interpolated pixels, and an HRS orthoimage with a 5 m resolution. The imagery had an absolute horizontal accuracy of 30 m root-mean-square (RMS), and the campaign resulted in DEMs covering most major ice caps and outlet glaciers (Korona and others, 2009; Exelis Visual Information Solutions, 2011). The ones used here were acquired on 4 August 2007 and 2 August 2008 for JI and on 27 July 2007 and 21 September 2008 for KL. They were manually edited using ENVI in which cloud and rock masks were applied, and the datum was changed from the Earth Gravitational Model 1996 (EGM96) geoid to the World Geodetic System 1984 (WGS84) ellipsoid. The spatial structure of errors was not accounted for.

2.2. ICESat

The spaceborne laser measurements are conducted using the Geosciences Laser Altimeter System (GLAS) on board ICESat. When the emitted pulses intersect the surface, a circular spot with a diameter of ~65 m is illuminated, and the along-track distance between two such consecutive footprints is 172 m. The data come from the GLAS/ICESat Antarctic and Greenland Ice Sheet Altimetry Data product (GLA12), release 31, and are downloaded from the US National Snow and Ice Data Center (NSIDC) website (Zwally and others, 2010). The elevation error is 10–15 cm and the datum is the TOPEX/Poseidon ellipsoid (Zwally and others, 2002; Schutz and others, 2005). A tidal saturation correction has been applied to data, and the reference surface is changed to the WGS84 ellipsoid. In order to use the data acquired closest in time to the SPOT dates, laser

campaigns 3I and 3K are selected. They span the periods October–November 2007 and October 2008, respectively.

2.3. ATM

The ATM is a lidar instrument flown on board an aircraft flying at typical altitudes of 400–500 m. The measurements are conducted with a laser altimeter conically scanning the ground below the aircraft. The frequency is 20 Hz, and the off-nadir scan angle of 15° illuminates a cone with a swath width of ~140 m. The footprint size is 1–3 m and the separation distance between consecutive footprints is ~2 m. The ATM instrument is mainly flown over coastal areas of high interest such as outlet glaciers known to experience large or rapid surface changes. Ground tracks are often repeated in order to observe intermediate changes, and with the aid of GPS and inertial navigation systems a minimum of 50% overlap with previous ground tracks is ensured (Krabill and others, 2002; Krabill, 2010).

The ATM data are referenced to the WGS84 ellipsoid and have an elevation error of 10–15 cm. Slope adjustment is performed using the ICESat (Institute for Computational Earth System Science, Santa Barbara, CA, USA) slopes. Given the SPOT dates for both observation years, 2007 ATM data are from May while the data for 2008 are from June/July at JI and July at KL.

3. METHOD FOR ESTIMATING ELEVATION CHANGES

When combining stereoscopic DEMs with altimetry, planimetric and elevation-dependent errors make it necessary to co-register the former to the latter in order to ensure that the observations represent the same location on the surface (Miller and others, 2009; Nuth and Kääb, 2011). By correcting for these offsets, the DEM surface is moved in space to fit the altimeter data, and the high spatial resolution of the imagery can then be used to extrapolate elevations not only along the altimeter flight lines but also in between. Having moved the DEMs from each year to fit the corresponding altimeter data, normally distributed residuals between the DEM and altimeter elevations are found at the altimeter points. As the datasets are not entirely contemporaneous, the residuals will contain information on the possible intermediate surface elevation changes occurring as a result of the different acquisition times. The remaining signal is believed to result from a bias in the SPOT DEMs (Korona and others, 2009). Applying the linear, unbiased estimators kriging and optimal linear estimation (OLE) to spatially interpolate the residuals to cover the entire observation area, the co-registered DEM surfaces can thus be corrected through information on the elevation difference between the datasets, and updated elevation maps can be produced. The resolution of the interpolation is 100 m, corresponding to the spatial variability of surface changes by shear margins and narrow ice streams such as outlet glaciers. By subtracting the 2007 elevations from those in 2008, the intermediate elevation changes and corresponding error estimates can be derived. Examples of input DEM and altimeter elevations are shown in Figure 1; the 2008 SPOT DEM is not shown due to its similarity with the 2007 image.

3.1. Registration and correction

We first downscale the spatial resolution of the DEMs from 40 m to 100 m using bilinear interpolation, after which we

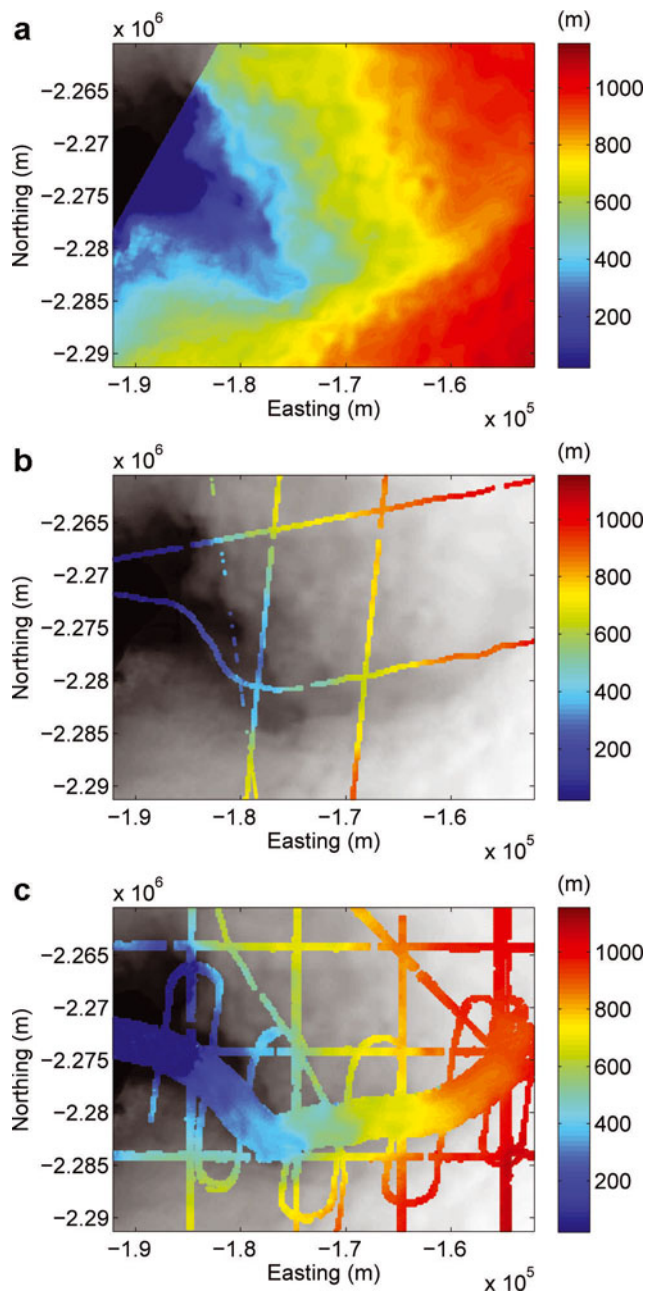


Fig. 1. Input DEM and altimeter surface elevations from the outlet of JI: (a) SPOT 5 DEM elevations acquired on 4 August 2007; (b) ICESat and ATM elevations from May and October/November 2007; and (c) ATM elevations from June/July 2008. No ICESat data were available for the latter period.

co-register the DEM from each year to the corresponding altimeter point cloud using a least-squares approach similar to that employed by Nuth and Kääb (2011). This minimizes planimetric offsets and elevation-dependent biases, thereby reducing the offsets between the surfaces and making the DEM elevations correspond to the altimeter points. Errors from this assumption are represented by the nugget effect in the kriging semivariogram and an input standard deviation in OLE.

Regarding Figure 2a, the planimetric biases between the DEM and altimeter surfaces, represented by $Z(x, y)$ and $z(x, y)$, respectively, can be described by the offset vector $\vec{\alpha}$ and the surface slope θ . The offset vector consists of both horizontal (α_{xy}) and vertical (α_z) contributions, and assuming

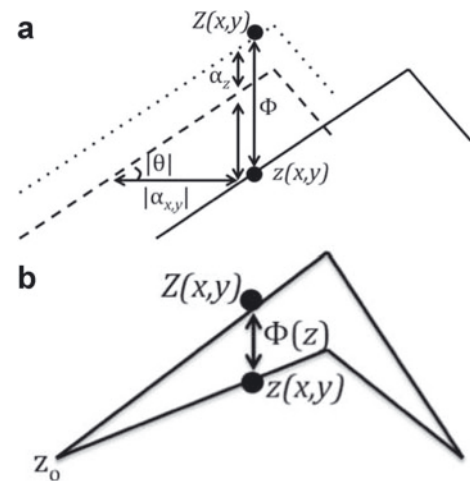


Fig. 2. Planimetric and elevation-dependent corrections necessary to apply when combining stereoscopic DEMs ($Z(x, y)$) with altimeter data ($z(x, y)$). (a) Planimetric offset. The total positional offset, Φ , is given as the sum of the contributions from the product of the horizontal offset, $|\alpha_{xy}|$, with the surface slope, θ , and the vertical offset, α_z . (b) Principle behind the elevation-dependent offset.

a constant surface slope over the distance $|\alpha_{xy}|$, the total vertical offset between the DEM and altimeter surfaces is

$$\begin{aligned}\Phi &= Z(x, y) - z(x, y) \\ &= \alpha_x \tan(\theta_x) + \alpha_y \tan(\theta_y) + \alpha_z \\ &= \alpha \cdot x + \epsilon\end{aligned}$$

where the model residual is given by ϵ .

By iteratively minimizing the offsets and discarding outliers greater than 2σ from the mean, the DEM is shifted in space until α reaches a minimum. The minimum value is chosen to be 1 m, and the result is a minimized root-mean-square error (RMSE) between the datasets. Following planimetric correction, we remove any elevation-dependent bias (Fig. 2b), which is assumed linear, through least-squares regression between the elevation and Φ . The result is the DEM adjusted to the best fit, in a least-squares sense, with the altimeter data. By subtracting the altimeter elevations from the DEM observations in the points (x, y) , the residuals are found to be normally distributed around a mean of 0 m (Fig. 3a and b).

3.2. Spatial interpolation

Following least-squares adjustment, we expand on the approach of Nuth and Kääb (2011) in order to further improve the DEM through interpolation and extrapolation of the residual differences with the altimeter elevations. Residuals that exceed the DEM elevation errors of approximately ± 12 m are treated as outliers and discarded, while geostatistical techniques are used to spatially interpolate the remaining residuals to cover the entire observation area. This allows one to gain a full overview of the offset introduced due to the different acquisition times of the SPOT image relative to the ATM and ICESat data. The interpolation gives both interpolated residuals, dz_{est} , and error variances. Taking the square root of the latter yields the RMSE, dz_{sig} . Linearly interpolating the adjusted DEM to the prediction points gives Z_{intp} , and the final, corrected, elevations are then found as

$$Z_{\text{new}} = Z_{\text{intp}} - (dz_{\text{est}} + dz_{\text{sig}}) \quad (1)$$

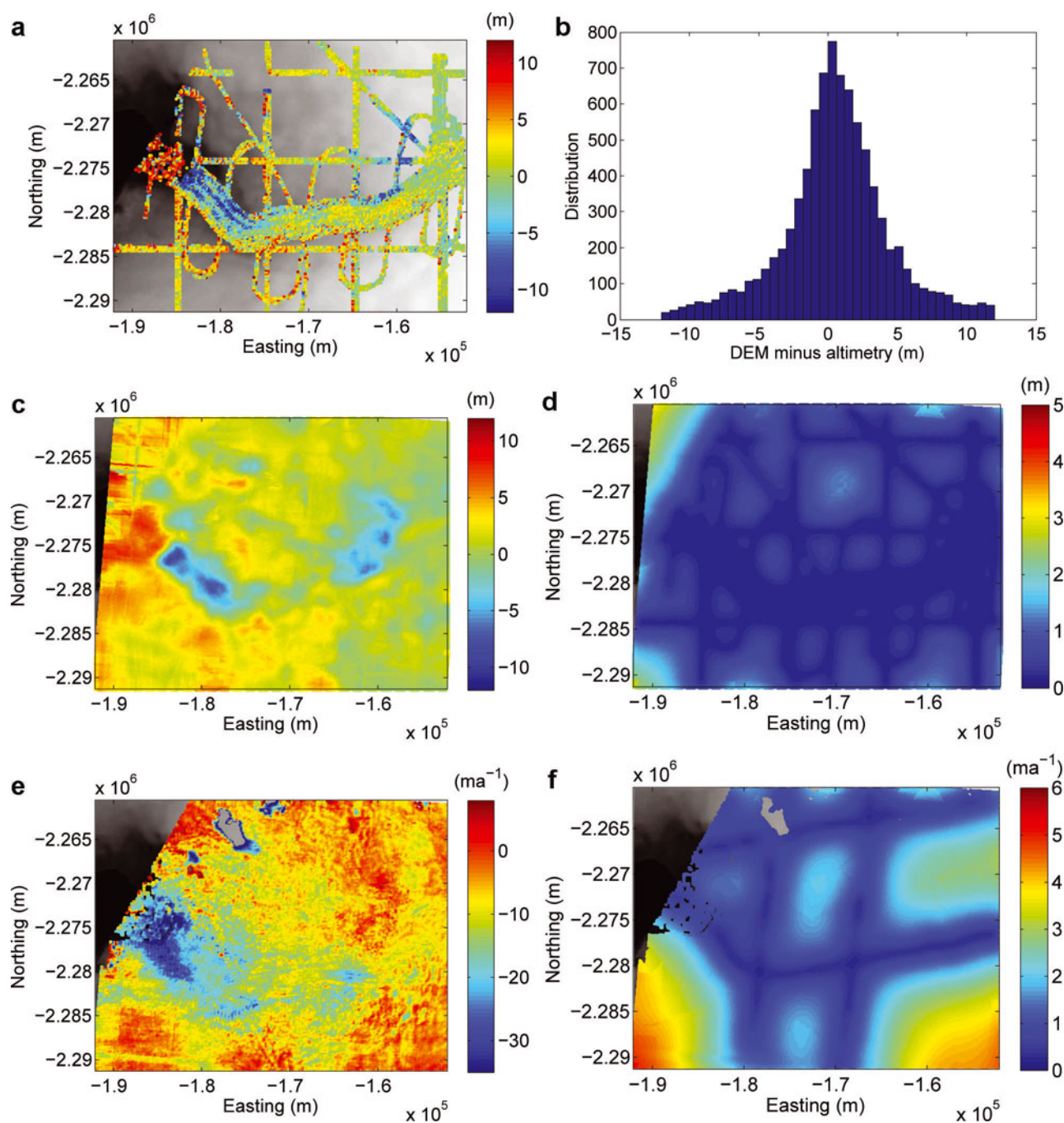


Fig. 3. Input data and results from OLE. (a) 2008 residuals given as DEM minus altimeter elevations in the altimeter observation points. The red areas show regions where the DEM elevations are higher, and the blue where they are lower. (b) The residuals' distribution in a histogram. (c, d) OLE interpolation values (c) and errors (d). (e, f) Using the 2007 and 2008 interpolation values to correct the corresponding DEMs, the intermediate surface elevation changes (e) and error estimates (f) are found.

By directly differencing the 2007 and 2008 elevations and converting the results to ma^{-1} , the intermediate elevation changes, dH/dt , are found.

Multiple interpolation methods are tested in order to find the one providing the most realistic result, i.e. prediction values that reproduce the residuals as accurately as possible without also producing a too smooth surface between the observation points. The methods are simple and ordinary kriging as well as OLE in the form of least-squares collocation (Hofmann-Wellenhof and Moritz, 2005). Kriging is performed using the MATLAB toolbox mGstat while OLE is performed with the Fortran-based GRAVSOFT program GEOGRID (Forsberg and Tscherning, 2008; Hansen, 2011).

A spherical semivariogram or a second-order Markov covariance model, respectively, is applied to the residuals found for each observation area for each year. All methods are linear, unbiased estimators, which minimize the estimation variance and return the input observation values for the observation points. In the case of a second-order stationary system, where the mean, variance and covariance are spatially constant, the methods are linked through the relation

$$\gamma(\vec{h}) = C(\vec{0}) - C(\vec{h}) \quad (2)$$

where $\gamma(\vec{h})$ is the semi-variance, $C(\vec{0})$ the variance, $C(\vec{h})$ the covariance and \vec{h} is the distance between two observations,

Table 1. Statistics on residuals (Φ) and interpolation results after applying optimal linear estimation to obtain dZ_{est} and dZ_{sig}

Glacier	Result	Year 2007	Year 2008
		m	m
Jakobshavn	mean(Φ)	0.2	0.5
	mean(dZ_{est})	0.5	1.3
	min(dZ_{sig})	0.2	0.2
	max(dZ_{sig})	4.6	3.2
Kangerdlugssuaq	mean(Φ)	-0.8	0.1
	mean(dZ_{est})	-0.5	0.1
	min(dZ_{sig})	0.2	0.2
	max(dZ_{sig})	3.6	4.1

i.e. the lag distance. If two measurements are conducted in close proximity to each other, they are assumed to have similar values. For a small lag, they are thus highly correlated, in which case the covariance is high and the semi-variance low.

For both methods, data errors are included by adding a semivariogram or variance-covariance matrix to the observations. We do not, however, create different semivariograms or variance-covariance matrices depending on the surface type as has been suggested by Rolstad and others (2009). They found different semivariogram parameters for steep and flat blue ice, snow and bedrock, respectively, as the surface type determines the spatial correlation between observations spaced by $\gamma(\vec{h})$. Data clustering is accounted for through a weighting based on the data configuration and their respective covariances/semi-variances rather than the actual observation values. Note that SK and OLE are essentially two ways of performing the same calculations (Dermanis, 1984; Hofmann-Wellenhof and Moritz, 2005; Nielsen, 2009).

4. RESULTS

Having spatially interpolated the residuals, similar results are found from the three techniques. A few differences are, however, evident, for example at JI where generally lower OLE errors ranging from ± 0.3 to 5.2 m a^{-1} are obtained compared to the kriging errors, which range from ± 3.6 to 7.6 m a^{-1} . Furthermore, kriging yields unrealistically smooth interpolation surfaces, while SK and OLE produce different results in spite of being constructed from the same set of equations. These differences are explained by the covariance model being of better quality than the variogram model, since the former implements the covariances directly while the latter uses a spherical semivariogram model fitted to the empirical values and thus does not include the residuals' oscillation above and below 0 m. The results presented in the following are therefore based on OLE.

An example of the residuals for the 2008 data at JI is shown in Figure 3a and b, while Figure 3c and d show the OLE interpolation values and RMSE, respectively. Table 1 summarizes the results in numbers. During the registration, the horizontal and vertical offsets are reduced from the decimeter level to the cm level, and during this process observations for which the residuals exceed the DEM errors of $\sim 12 \text{ m}$ are treated as outliers and discarded. This reduces the number of data points (Fig. 3a relative to Fig. 1c) and

Table 2. Surface elevation change (m a^{-1}) results from the two glaciers. The last column gives the elevation change error found by applying quadratic summation to the 2007 and 2008 interpolation errors

Glacier	dH/dt (terminus)	dH/dt (flow channel)	dH/dt (remaining surface)	$\sigma_{dH/dt}$
Jakobshavn	-35 to -30	-25 to -10	-5 to 3	± 0.3 to 5.2
Kangerdlugssuaq	-25 to -8	-20 to 0	0 to 5	± 0.3 to 5.1

results in residuals normally distributed around zero. The largest negative offsets are found along the flow channel where the largest surface changes occur. As the August DEM is registered to ATM data from June/July, the intermediate lowering of the surface will yield negative residuals when subtracting the altimeter observations from the DEM. Further inland, the offsets are closer to zero, while some positive values are also found. These can be explained by errors in the DEMs (Korona and others, 2009). The RMSE ranges from 0.2 to 4.6 m, with the lowest values coinciding with the position of the altimeter points, and the greater the distance to these, the larger the error. It is found that for flights $\sim 10 \text{ km}$ apart, the errors range from 0.2 to 2 m, while when the distance between ground tracks halves, the error approximately halves accordingly. As will become clearer from the elevation change maps presented below, this relation is important when planning the spatial density of airborne flights in order to estimate surface changes in areas of varying topography, such as at outlet glaciers.

The surface elevations and elevation changes are found using Eqn (1), and as data errors are taken into account during the interpolation, Gaussian quadratic summation can be applied to the 2007 and 2008 RMSE values to give the dH/dt error estimates, $\sigma_{dH/dt}$. The results are presented in Figures 3e and f and 4a and b as well as in Table 2. The data gaps in the figures result from errors as well as the application of cloud and rock masks during the initial manual editing of the DEMs. For JI (Fig. 3e), a large area with $dH/dt \approx -35 \text{ m a}^{-1}$ marks the glacier basin. Surrounding this, the flow channel is distinguishable with dH/dt between -25 and -10 m a^{-1} and values increasing further inland. This large lowering agrees well with the mass loss reaching a maximum of 34 Gt a^{-1} by the end of 2007, after which it fluctuates between 25 and 33 Gt a^{-1} (Howat and others, 2011). At higher elevations further east, the pattern of dH/dt changes with values of approximately or slightly above 0 m a^{-1} , indicating a steady or slowly rising surface. The errors (Fig. 3f) range from ± 0.3 to 5.2 m a^{-1} , the lowest values being found nearest to the altimeter ground tracks, after which they increase with distance from there.

At KL (Fig. 4a), negative elevation changes are found throughout most of the observation area, making the flow pattern clearly noticeable. The glacier basin and the area north of it experienced a large lowering of dH/dt between -25 and -10 m a^{-1} . Higher elevations to the east and southwest are less affected by recent changes in ice flow, so $dH/dt \approx 0 \text{ m a}^{-1}$. The positive values scattered around the flow channel and drainage basin are believed to result from melt lakes on the ice as well as a major retreat ending in

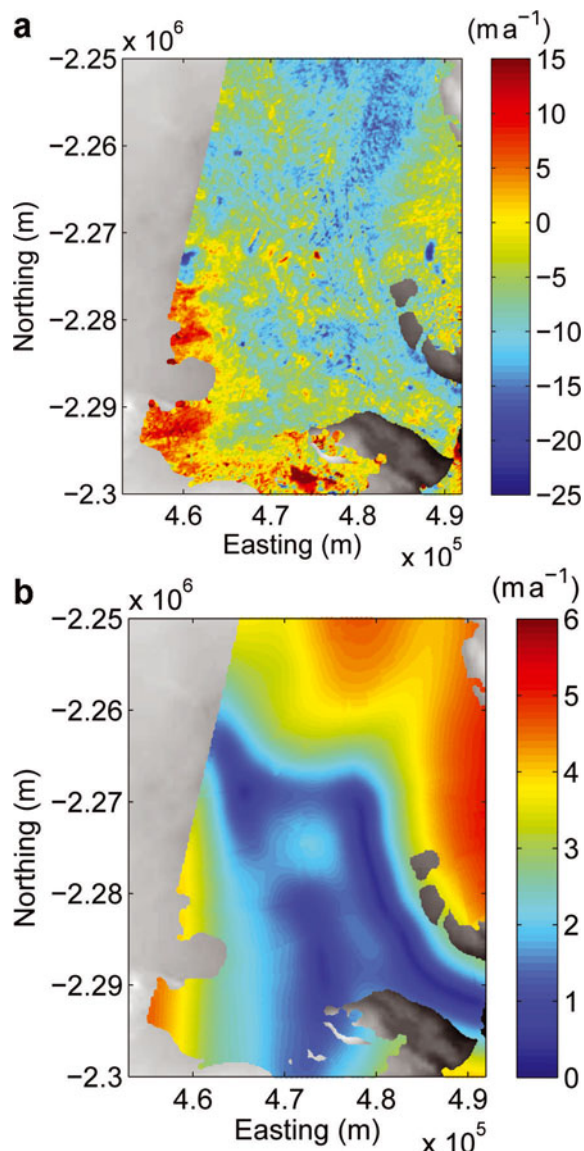


Fig. 4. Surface elevation changes (a) and error estimates (b) from KL from 2007 to 2008.

2005–06, after which the front stabilized (Howat and others, 2011). The errors span ± 0.3 – 5.1 m a^{-1} (Fig. 4b). The minimum is found in the vicinity of approximately overlapping altimeter ground tracks, i.e. in the glacier basin with the minimum values depicting the overlap. Unfortunately, there are no observations in the area immediately north/northwest of the basin where $dH/dt < 0 \text{ m a}^{-1}$. This is reflected in generally higher errors, i.e. $\sigma_{dh/dt} = \pm 2.9$ – 5.1 m a^{-1} . It also explains the greater number of higher errors at KL than at JI where altimeter data cover a larger part of the observation area.

5. DISCUSSION

Both kriging and OLE are linear, unbiased estimators that take data clustering into account when spatially interpolating a set of measurements. Thus, the interpolation depends on the spatial distribution of data rather than their actual values, and the formation of a spatially varying mean of the observation values is allowed. The results indicate a clear relationship between the distribution of altimeter data

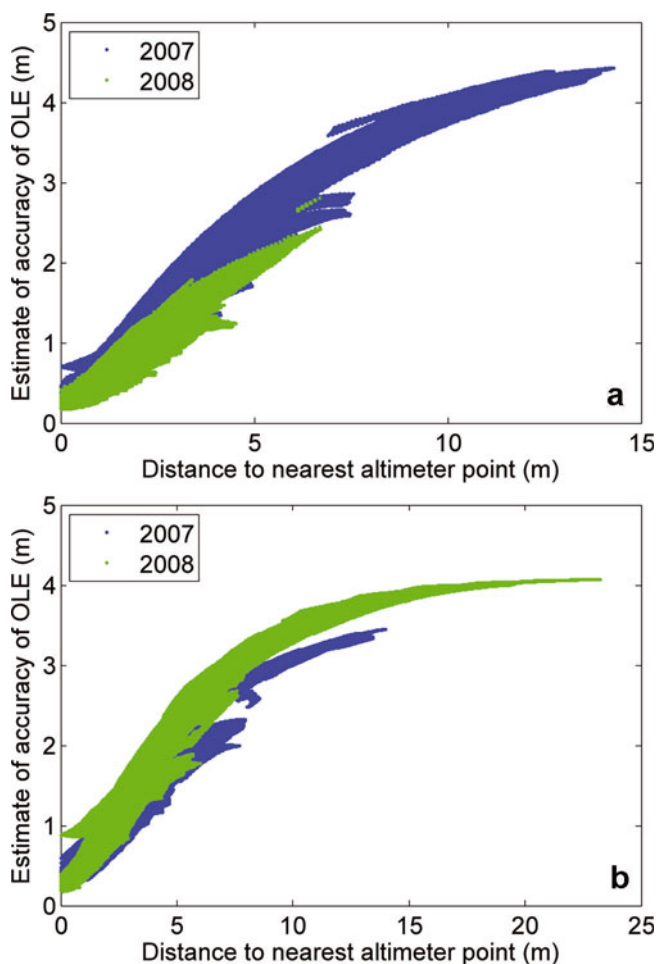


Fig. 5. Estimate of accuracy of OLE as a function of the distance to the closest altimeter point. As the accuracy estimates are used to find the surface elevation change errors, this relationship translates directly. (a) JI and (b) KL.

and the errors: the denser the grid of observations, the more accurate the predictions based on the neighbourhood, and the lower the errors. Figure 5 illustrates this relationship for the OLE interpolation errors, and as these are used to produce the dH/dt errors, this distance dependence translates directly. This observation is crucial in planning future airborne surveys as it can be used to ensure that flights are carried out in grids dense enough to ensure minimum errors. The reason for the low errors relative to the data errors is the referencing of the DEMs to altimeter observations agreeing in time and space, as well as OLE being based on a well-defined covariance model which takes data errors into account. The spatial structure of the DEM errors is not accounted for, however, as we only had point-wise errors in the estimation points. This may explain the positive residuals found at JI when registering the August 2008 DEM to June/July ATM data. Another possible explanation is that we have not accounted for different surface types, such as steep/flat blue ice and snow, giving different semivariograms/variance-covariance matrices (Rolstad and others, 2009). This changes the parameters in the models used for the interpolation if, for example, steep slopes indicate less spatial correlation between the observation points. In spite of this, our results agree well with those obtained by Howat and others (2011), who estimated surface mass-balance changes for the period 2000–10 for Helheim, KL and JI using

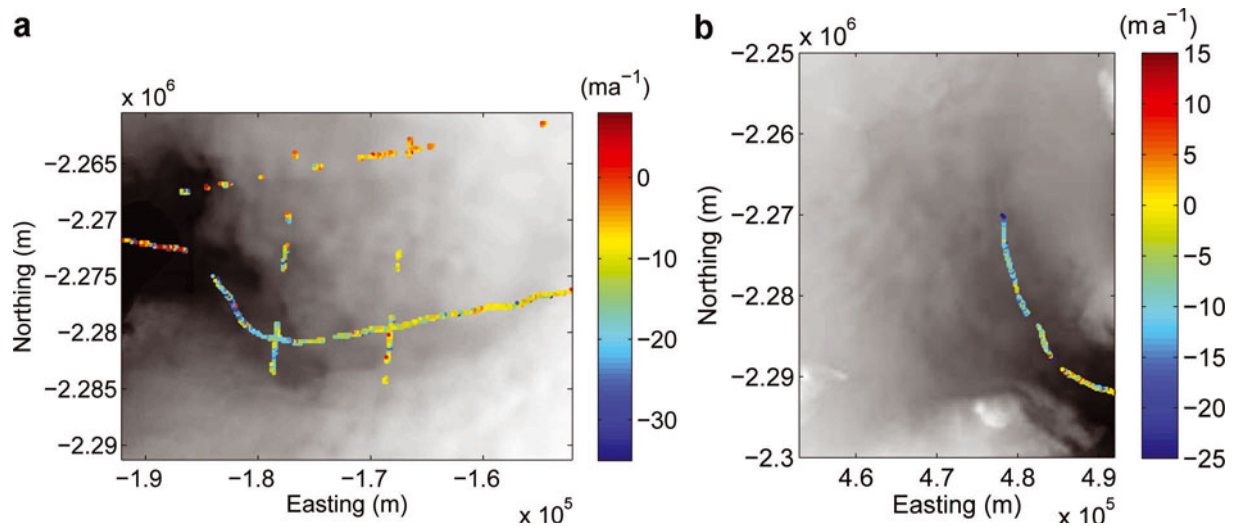


Fig. 6. ATM elevation changes between May 2007 and June/July 2008 for validation purposes: (a) JI and (b) KL.

the Regional Atmospheric Climate Model version 2 (RACMO2) as described by Ettema and others (2009, 2010). Howat and others (2011) found that a major front retreat ended in 2005–06, after which the front stabilized. This supports the patchy thickening of KL's glacier basin. When considering elevation changes derived from ATM only (Fig. 6), we observe a trend similar to ours: a lowering of JI's trunk of $\sim 25 \text{ m a}^{-1}$, $\sim 10 \text{ m a}^{-1}$ further up the channel, and values of $\sim 0 \text{ m a}^{-1}$ and below at higher elevations north of the flow channel. We thus have confidence in our results.

As the laser data and DEMs are not acquired at exactly the same time of the year, an error is introduced due to the seasonal signal of the ice. However, as the DEMs are co-registered to altimeter ICESat and ATM data, several limitations emerge, which complicate or prevent the acquisition of all the data simultaneously: ICESat's orbit limited the spatial and temporal distribution of flights, and ATM is flown according to logistics, weather and target priorities. Furthermore, the SPIRIT campaign was of short duration and only focused on certain parts of the Greenland ice sheet. As the JI DEMs are co-registered to altimeter data acquired from April to October and the DEMs from KL are separated by 14 months, it is not valid to assume that the seasonal elevation cycle was eliminated from the difference data. One path to mitigating the effects arising from surface processes is through the use of a coupled surface energy and meteorological reanalysis model such as that by Van den Broeke and others (2010). By applying such an approach, even sharper Gaussian curves will be found than those from this analysis, (Fig. 3b). In spite of this, part of the information contained in the residuals is exactly the offset resulting from different temporal resolutions. Spatially interpolating the offsets over the entire observation area demonstrates the strength of our model: it provides the ability to identify and correct offsets using geostatistical interpolation, thereby improving the DEM elevations and DEM differences.

The combination of datasets described here may be generally applicable to many other data sources (e.g. Envisat, CryoSat-2 and the Advanced Spaceborne Thermal Emission and Reflection Radiometer (ASTER)). Once airborne and validated, data from ICESat-II can also be employed. CryoSat-2 data are becoming available to the scientific community at the time of writing, while Envisat

operated from 2002 until April 2012, yielding a vast number of data from its 35 day repeat track period. Although it is necessary to account for backscattering effects and the radar signal's penetration into the firn, work is ongoing in order to fully understand the implications, such as through CryoVex, the CryoSat-2 validation campaign carried out using both laser and radar altimetry (Drinkwater and Rebhan, 2003). NASA's Land, Vegetation, and Ice Sensor (LVIS) has been flown over most of Greenland's west and southeast coasts as part of Operation IceBridge, and GPS receivers are deployed on the ice by outlet glaciers such as JI and Russell Glacier. As they provide continuous and very accurate position and elevation estimates, the inclusion of such data will be beneficial for ensuring consistently high-accuracy estimates (Joughin and others, 2008; Shepherd and others, 2009; Khan and others, 2010). Satellite imagery is available from, for example, the ASTER sensor on board the Terra satellite. Such data have been available since 1999, and numerous projects aimed at estimating surface changes in ice-covered regions have been conducted (Howat and others, 2007; Kääh, 2008). Thus, although the SPIRIT campaign has finished and ICESat is no longer operating, there is a possibility of continuously constraining DEMs using more accurate datasets to increase the spatial resolution and decrease the errors of surface elevation maps, particularly in areas of a rough surface topography.

6. CONCLUSIONS

This work focused on developing a method for estimating elevation changes with a high spatial resolution in areas with rapid surface changes such as outlet glaciers. This involved a combination of stereoscopic DEMs from SPOT 5 and laser altimeter data from ICESat and ATM, and the test regions were the two Greenlandic outlet glaciers Jakobshavn Isbræ and Kangerdlugssuaq over the period 2007–08. The goal was to co-register the DEMs to altimeter data as they agreed in time and space. The altimeter elevation error was one order of magnitude smaller than that of the DEM, 10–15 cm, thus representing a good approximation of the true surface. By moving the DEM in space until it agreed with the laser data and applying geostatistical interpolation in the form of optimal linear estimation, it became possible to correct the

DEMs for the offsets relative to the altimeter surfaces. In this way, elevation maps were produced with a spatial resolution of 100 m and elevation errors no higher than ± 4.6 m (Jl 2007). Simple and ordinary kriging were also applied, but led to significantly poorer results. The method allowed detailed information to be obtained regarding the surface topography throughout the observation areas, i.e. not only along but also between the altimeter flight lines and ground tracks. It also reduced the estimation errors noticeably, particularly in the vicinity of altimeter observations. For flights ~ 10 km apart, the errors ranged from ± 0.2 to 2 m, and when halving the distance between ground tracks, the error halved accordingly.

By differencing two elevation maps, the temporal surface elevation changes were mapped, and for the given observation period a lowering of the terminus region and flow channel was observed for both glaciers. For Jl, the terminus lowered by -35 to -30 m. The flow channel lowered by -25 to -10 m a^{-1} , while the surrounding higher-elevation areas were approximately unchanged. For Kl, part of the terminus lowered at rates of 20 – 25 m a^{-1} while the flow channel experienced a lowering of approximately -18 to -5 m a^{-1} . The remaining surface rose by a few m a^{-1} . The elevation change errors ranged from ± 0.3 to 5.2 m a^{-1} for Jl and ± 0.3 to 5.1 m a^{-1} for Kl, and as was the case in the interpolation the smallest errors were found in the vicinity of altimeter observations. A significant result was this strong dependence of the size of the errors on the position of the altimeter data: As the density of altimeter observations increased, the errors decreased significantly. Thus, as satellite orbits cannot be changed, for example, to observe short-term surface changes in specific areas, and because exact repeat tracks are rare, this relationship between flight lines and estimation errors is of great importance for airborne flight planning. Previous ATM ground tracks are often re-flown with a $>50\%$ overlap (Krabill and others, 2002). When combined with knowledge of the error distribution, the combination of stereoscopic imagery and laser altimeter data, particularly acquired during airborne campaigns, enables continuous mapping of both accurate surface elevations and elevation changes in areas of rapidly changing ice surfaces.

ACKNOWLEDGEMENTS

The ICESat and ATM data were downloaded from the NSIDC website, and the SPOT 5-HRS imagery was obtained as part of the SPIRIT campaign launched by CNES, SPOT Image and LEGOS. J.F. Levinsen acknowledges I.M. Howat for receiving her into his research group at the School of Earth Sciences at The Ohio State University. The stay was made possible through a Fulbright scholarship. We thank the reviewers for constructive comments, which led to a significant improvement of the manuscript.

REFERENCES

- Berthier E and Toutin T (2008) SPOT5-HRS digital elevation models and the monitoring of glacier elevation changes in North-West Canada and South-East Alaska. *Remote Sens. Environ.*, **112**(5), 2443–2454 (doi: 10.1016/j.rse.2007.11.004)
- Bouillon A, Bernard M, Gigord P, Orsoni A, Rudowski V and Baudoin A (2006) SPOT 5 HRS geometric performances: using block adjustment as a key issue to improve quality of DEM generation. *ISPRS J. Photogramm. Remote Sens.*, **60**(3), 134–146 (doi: 10.1016/j.isprsjprs.2006.03.002)
- Carabajal CC and Harding DJ (2005) ICESat validation of SRTM C-band digital elevation models. *Geophys. Res. Lett.*, **32**(22), L22S01 (doi: 10.1029/2005GL023957)
- Dermanis A (1984) Kriging and collocation: a comparison. *Manuscr. Geodaet.*, **9**(3), 159–167
- Drinkwater M and Rebhan H eds. (2003) *Cryosat science report*. (ESA SP-1272) European Space Agency/European Space and Technology Centre, Noordwijk
- Ettema J and 6 others (2009) Higher surface mass balance of the Greenland ice sheet revealed by high-resolution climate modelling. *Geophys. Res. Lett.*, **36**(12), L12501 (doi: 10.1029/2009GL038110)
- Ettema J, Van den Broeke MR, Van Meijgaard E, Van de Berg WJ, Box JE and Steffen K (2010) Climate of the Greenland ice sheet using a high-resolution climate model: Part 1: evaluation. *Cryosphere*, **4**(4), 511–527 (doi: 10.5194/tc-4-511-2010)
- Exelis Visual Information Solutions (2011) *ENVI*. Exelis Visual Information Solutions <http://www.exelisvis.com/ProductsServices.aspx>
- Forsberg R and Tscherning CC (2008) *An overview manual for the GRAVSOFIT Geodetic Gravity Field Modelling Programs*, 2nd edn. National Space Institute (DTU Space) and Niels Bohr Institute, University of Copenhagen, Copenhagen
- Hansen TM (2011) *mGstat: a geostatistical Matlab toolbox* <http://mgstat.sourceforge.net/>
- Hofmann-Wellenhof B and Moritz H (2005) *Physical geodesy*. Springer, Vienna
- Howat IM, Joughin IR and Scambos TA (2007) Rapid changes in ice discharge from Greenland outlet glaciers. *Science*, **315**(5818), 1559–1561 (doi: 10.1126/science.1138478)
- Howat IM, Ahn Y, Joughin I, Van den Broeke MR, Lenaerts JTM and Smith B (2011) Mass balance of Greenland's three largest outlet glaciers, 2000–2010. *Geophys. Res. Lett.*, **38**(12), L12501 (doi: 10.1029/2011GL047565)
- Joughin I, Das SB, King MA, Smith BE, Howat IM and Moon T (2008) Seasonal speedup along the western flank of the Greenland Ice Sheet. *Science*, **320**(5877), 781–783 (doi: 10.1126/science.1153288)
- Kääb A (2008) Glacier volume changes using ASTER satellite stereo and ICESat GLAS laser altimetry: a test study on Edgeøya, Eastern Svalbard. *IEEE Trans. Geosci. Remote Sens.*, **46**(10), 2823–2830 (doi: 10.1109/TGRS.2008.2000627)
- Khan SA, Wahr J, Bevis M, Velicogna I and Kendrick E (2010) Spread of ice mass loss into northwest Greenland observed by GRACE and GPS. *Geophys. Res. Lett.*, **37**(6), L06501 (doi: 10.1029/2010GL042460)
- Korona J, Berthier E, Bernard M, Rémy F and Thouvenot E (2009) SPIRIT. SPOT 5 stereoscopic survey of polar ice: reference images and topographies during the fourth International Polar Year (2007–2009). *ISPRS J. Photogramm. Remote Sens.*, **64**(2), 204–212 (doi: 10.1016/j.isprsjprs.2008.10.005)
- Krabill WB (2010) *IceBridge ATM L2 Icessn elevation, slope, and roughness*. NASA Distributed Active Archive Center, National Snow and Ice Data Center, Boulder, CO. Digital media: <http://nsidc.org/data/docs/daac/icebridge/ilatm2/>
- Krabill WB and 8 others (2002) Aircraft laser altimetry measurement of elevation changes of the Greenland ice sheet: technique and accuracy assessment. *J. Geodyn.*, **34**(3–4), 357–376 (doi: 10.1016/S0264-3707(02)00040-6)
- Miller PE and 6 others (2009) Assessment of glacier volume change using ASTER-based surface matching of historical photography. *IEEE Trans. Geosci. Remote Sens.*, **47**(7), 1971–1979 (doi: 10.1109/TGRS.2009.2012702)
- Nielsen AA (2009) *Geostatistics and analysis of spatial data*, Technical University of Denmark (DTU), Lyngby http://www2.imm.dtu.dk/pubdb/views/publication_details.php?id=5177
- Nuth C and Kääb A (2011) Co-registration and bias corrections of satellite elevation data sets for quantifying glacier thickness

- change. *Cryosphere*, **5**(1), 271–290 (doi: 10.5194/tc-5-271-2011)
- Rolstad C, Haug T and Denby B (2009) Spatially integrated geodetic glacier mass balance and its uncertainty based on geostatistical analysis: application to the western Svaritsen ice cap, Norway. *J. Glaciol.*, **44**(192), 666–680 (doi: 10.3189/002214309789470950)
- Schenk T, Csatho B, Van der Veen CJ, Brecher H, Ahn Y and Yoon T (2005) Registering imagery to ICESat data for measuring elevation changes on Byrd Glacier, Antarctica. *Geophys. Res. Lett.*, **32**(23), L23S05 (doi: 10.1029/2005GL024328)
- Schutz BE, Zwally HJ, Shuman CA, Hancock D and DiMarzio JP (2005) Overview of the ICESat Mission. *Geophys. Res. Lett.*, **32**(21), L21S01 (doi: 10.1029/2005GL024009)
- Shepherd A, Hubbard A, Nienow P, McMillan M and Joughin I (2009) Greenland ice sheet motion coupled with daily melting in late summer. *Geophys. Res. Lett.*, **36**(1), L01501 (doi: 10.1029/2008GL035758)
- Sørensen LS and 7 others (2011) Mass balance of the Greenland ice sheet (2003–2008) from ICESat data – the impact of interpolation, sampling and firn density. *Cryosphere*, **5**(1), 173–186 (doi: 10.5194/tc-5-173-2011)
- Thomas R, Frederick E, Krabill W, Manizade S and Martin C (2009) Recent changes on Greenland outlet glaciers. *J. Glaciol.*, **55**(189), 147–162 (doi: 10.3189/002214309788608958)
- Van den Broeke M, Bus C, Ettema J and Smeets P (2010) Temperature thresholds for degree-day modelling of Greenland ice sheet melt rates. *Geophys. Res. Lett.*, **37**(18), L18501 (doi: 10.1029/2010GL044123)
- Zwally HJ and 15 others (2002) ICESat's laser measurements of polar ice, atmosphere, ocean and land. *J. Geodyn.*, **34**(3–4), 405–445 (doi: 10.1016/S0264-3707(02)00042-X)
- Zwally HJ and 7 others. (2010) *GLAS/ICESat L2 Antarctic and Greenland Ice Sheet Altimetry Data, V031*. National Snow and Ice Data Center, Boulder, CO <http://nsidc.org/data/gla12.html>

MS received 27 June 2012 and accepted in revised form 23 January 2013